비선형 모델링과 외란 관측기를 이용한 Matrix Converter로 구동되는 유도전동기 센서리스 벡터제어의 성능 개선

論 文
53B-8-6

Performance Improvement of Sensorless Vector Control for Induction Motor Drives Driven By Matrix Converter Using Non-Linearity Compensation and Disturbance Observer

李 敎 範*
(Kyo-Beum Lee)

Abstract - This paper presents a new sensorless vector control system for high performance induction motor drives fed by a matrix converter with non-linearity compensation and disturbance observer. The nonlinear voltage distortion that is caused by commutation delay and on-state voltage drop in switching device is corrected by a new matrix converter modeling. The lumped disturbances such as parameter variation and load disturbance of the system are estimated by the radial basis function network (RBFN). An adaptive observer is also employed to bring better responses at the low speed operation. Experimental results are shown to illustrate the performance of the proposed system.

Key Words : Matrix converter, induction motor, sensorless vector control, non-linearity modeling and disturbance observer

1. INTRODUCTION

The induction motor drive fed by matrix converter is superior to the conventional inverter because of the lack of the bulky DC-link capacitors with limited life time, the bi-directional power flow capability, the sinusoidal input/output currents, and adjustable input power factor. Furthermore, because of the high integration capability and the higher reliability of the semiconductor structures, the matrix converter topology is recommended for extreme temperatures and critical volume/weight applications. However, a few of the practical matrix converters have been applied to induction motor drive system because the implementation of switch devices in the matrix converter is difficult and modulation technique and commutation control are more complicated than the conventional PWM inverter [1-3].

In order to realize a high performance control of induction motor drives fed by matrix converter, a matrix converter model for low speed operation and robust speed controller using disturbance observer are proposed in this paper. As for the conventional inverter to drive induction motors, several respective methods of non-linearity modeling for low speed operation are found in the literature [4-5]. On the contrary, research results on non-linearity modeling schemes for matrix converters are hardly reported. The nonlinear voltage distortion in the matrix converter in low speed operation is comprehensively investigated and these problems are resolved by online compensation using a new matrix converter modeling. To improve the low-speed operation performance, an adaptive full-order observer is employed for the estimation of the stator flux, the rotor speed, and the stator resistance over the wide speed operation region [6]. In addition, the lumped disturbances of the induction motor drive fed by matrix converter are approximated by a radial basis function network including parameter variations and external load disturbances [7]. Experimental results are presented to verify the effectiveness and feasibility of the proposed control system.

* 正 會 員 : PostDoc. Researcher, Institute of Energy Technology, Aalborg University, Denmark

接受日字 : 2004年 4月 6日
最終完了 : 2004年 7月 7日

2. SENSORLESS VECTOR OF INDUCTION MOTOR DRIVES FED BY MATRIX CONVERTER

2.1 CONTROL PRINCIPALS OF MATRIX CONVERTER

The main circuit of a matrix converter is shown in Fig. 1. There are the input filter, the bi-directional switches connected in a three-phase to three-phase matrix and a clamp circuit. The input LC filter is a second order low-pass topology, which is used to reduce the high-frequency ripple from the input current. The

clamp circuit consists of two diode bridges to connect the input and the output to a clamp capacitor, in order to protect the switches against possible over-voltages that appear during transient.

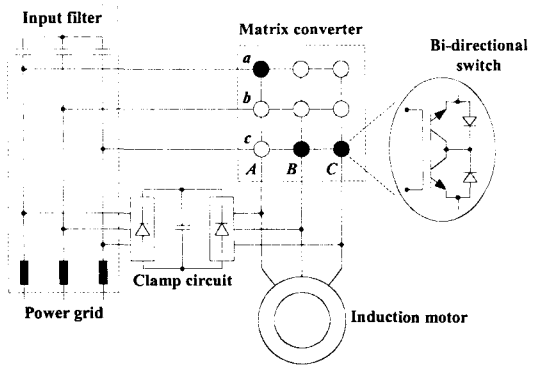

Fig. 1. The topology of a matrix converter drive

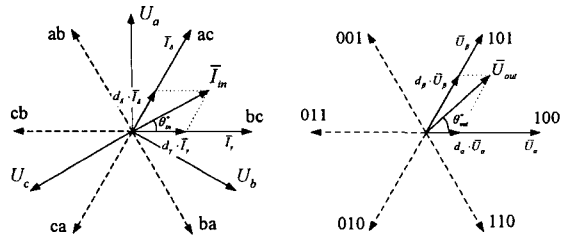

(a) (b)

Fig. 2. Generation of the reference voltage vectors using ISVM
(a) in the rectification stage, (b) in the inversion stage

provide a constant imaginary DC-link voltage per switching period and an inverter stage to produce the three output voltages.

The input current vector, I_{in} that corresponds to the rectification stage and the output voltage vector, U_{out} that corresponds to the inversion stage are the reference vectors (Fig. 2). The indirect space vector modulation uses a combination of the two adjacent vectors and a zero vector to produce the reference vector. The ratio between the two adjacent vectors duty cycle determines the magnitude of the reference vector. The duty cycles of the active switching vectors for the rectification stage, I_γ, I_δ are calculated with (1) and the duty cycle of the active switching vectors for the inversion stage, U_α, U_β are calculated with (2).

$$d_\gamma = m_I \sin\left(\frac{\pi}{3} - \theta_{in}^*\right) \text{ and } d_\delta = m_I \sin\theta_{in}^* \quad (1)$$

$$d_\alpha = m_U \sin\left(\frac{\pi}{3} - \theta_{out}^*\right) \text{ and } d_\beta = m_U \sin\theta_{out}^* \quad (2)$$

where, m_I and m_U are the rectification and inversion stage modulation indexes, θ_{in}^* and θ_{out}^* are the angles within their respective sectors of the input current and output voltage reference vectors (see Fig. 2).

To obtain a correct balance of the input currents and the output voltages in the same switching period, the modulation pattern should produce all combinations of the rectification $(\gamma-\delta-0)$ and the inversion $(\alpha-\beta-0)$ switching states, resulting in the following switching

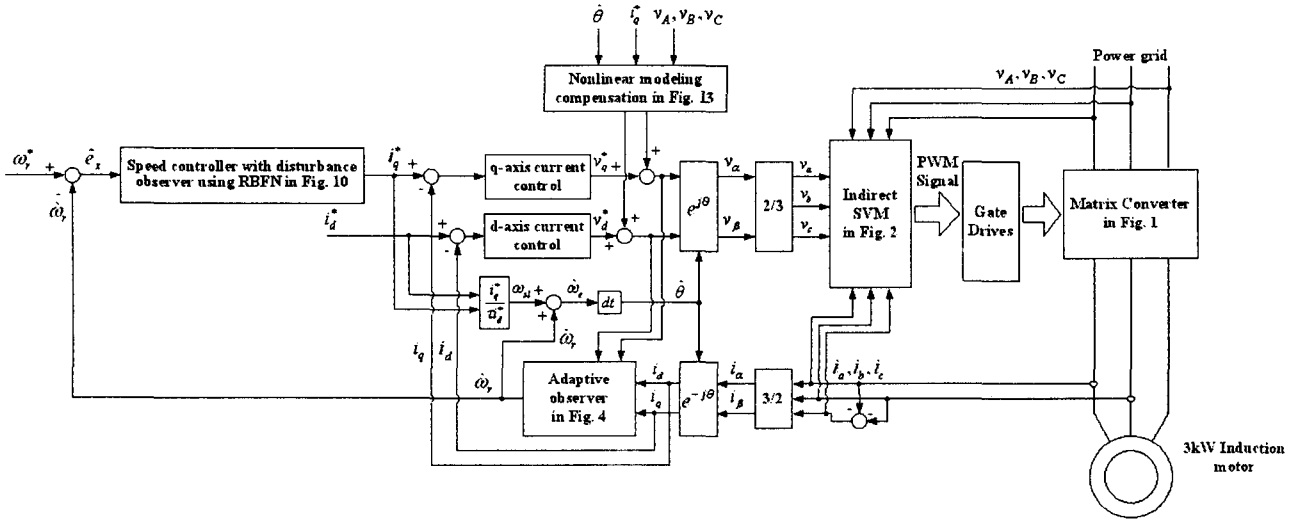

Fig. 3. The proposed sensorless vector control for induction motor drives fed by matrix converter

The most general modulation method for matrix converter is the Indirect Space Vector Modulation (ISVM), which considers the matrix converter as a two stage transformation converter: a rectification stage to

pattern: $\alpha\gamma-\alpha\delta-\beta\delta-\beta\gamma-0$. Therefore, each sequence duty cycle is a result of the cross products of the rectification and the inversion stage duty cycles, while the duration of the zero-vector is completing the

switching sequence as

$$d_{\alpha\gamma} = d_\alpha d_\gamma,\ d_{\alpha\delta} = d_\alpha d_\delta,\ d_{\beta\delta} = d_\beta d_\delta,\ d_{\beta\gamma} = d_\beta d_\gamma,$$
$$d_0 = 1 - (d_{\alpha\gamma} + d_{\alpha\delta} + d_{\beta\delta} + d_{\beta\gamma}). \quad (3)$$

The duration of each sequence is found by multiplying the corresponding duty cycle to the switching period.

The proposed control scheme of sensorless vector control for induction motor drives fed using a matrix converter is shown in Fig. 3, which consists of an adaptive observer for speed and rotor flux estimation, nonlinear modeling of matrix converter, and speed controller using radial basis function network disturbance observer [5-6].

2.2 SENSORLESS VECTOR CONTROL USING ADAPTIVE OBSERVER

In order to build a high performance speed sensorless vector control system for induction motors fed by matrix converter, accurate information on the motor speed, and the flux are required. An adaptive observer that offers good performance in a large speed range is employed to make a high performance drive. An adaptive observer makes use of the analytical model and allows the estimation of both the rotor speed and flux from the motor currents. Its implementation is relatively simple by means of DSP systems.

Equations required to implement the adaptive observer are describes as

$$\frac{d}{dt}\hat{X} = \hat{A}\hat{X} + BV + G\left(\hat{I}_s - I_s\right) \quad (4)$$

where,

$\hat{X} = [\hat{i}_{ds}\ \hat{i}_{qs}\ \hat{\lambda}_{dr}\ \hat{\lambda}_{qr}]^T$: Estimated values of stator current and rotor flux,

$V_s = [v_{ds}\ v_{qs}]^T$: Stator voltage,

$\hat{I}_s = [\hat{i}_{ds}\ \hat{i}_{qs}]^T$: Estimated values of stator current,

$I_s = [i_{ds}\ i_{qs}]^T$: Stator current,

$$\hat{A} = \begin{bmatrix} -\left(\frac{\hat{R}_s}{\sigma L_s} + \frac{1-\sigma}{\sigma\tau_r}\right) & 0 & \frac{L_m}{\sigma L_s L_r \tau_r} & \frac{L_m}{\sigma L_s L_r}\hat{w}_r \\ 0 & -\left(\frac{\hat{R}_s}{\sigma L_s} + \frac{1-\sigma}{\sigma\tau_r}\right) & -\frac{L_m}{\sigma L_s L_r}\hat{w}_r & \frac{L_m}{\sigma L_s L_r \tau_r} \\ \frac{L_m}{\tau_r} & 0 & -\frac{1}{\tau_r} & -\hat{w}_r \\ 0 & \frac{L_m}{\tau_r} & \hat{w}_r & -\frac{1}{\tau_r} \end{bmatrix},$$

$$B = \begin{bmatrix} \frac{1}{\sigma L_s} & 0 \\ 0 & \frac{1}{\sigma L_s} \\ 0 & 0 \\ 0 & 0 \end{bmatrix},\quad G = \begin{bmatrix} g_1 & g_2 & g_3 & g_4 \\ -g_2 & g_1 & -g_4 & g_3 \end{bmatrix}^T,$$

$\sigma = 1 - \frac{L_m^2}{L_s L_r}$: Leakage coefficient,

$\tau_r = \frac{L_r}{R_r}$: Rotor time constant,

$$g_1 = (k-1)\left\{-\left(\frac{\hat{R}_s}{\sigma L_s} + \frac{1-\sigma}{\sigma\tau_r}\right) - \frac{1}{\tau_r}\right.,$$

$$g_2 = (k-1)\hat{w}_r,$$

$$g_3 = (k^2-1)\left[\sigma L_s L_r\left(\frac{\hat{R}_s}{\sigma L_s} + \frac{1-\sigma}{\sigma\tau_r}\right) + \frac{L_m}{\tau_r} - \frac{\sigma L_s L_r (k-1)}{L_m}\left\{\left(\frac{\hat{R}_s}{\sigma L_s} + \frac{1-\sigma}{\sigma\tau_r}\right) - \frac{1}{\tau_r}\right\}\right],$$

$$g_4 = -\frac{\sigma L_s L_r (k-1)\hat{w}_r}{L_m},$$

R_s, R_r : Stator and rotor resistance,

L_s, L_r : Stator and rotor self inductance,

L_m : Mutual inductance.

$$\hat{w}_r = K_p\left(e_{ids}\hat{\lambda}_{qr} - e_{iqs}\hat{\lambda}_{dr}\right) + K_i\int\left(e_{ids}\hat{\lambda}_{qr} - e_{iqs}\hat{\lambda}_{dr}\right)dt \quad (5)$$

where $e_{ids} = i_{ds} - \hat{i}_{ds}$ and $e_{iqs} = i_{qs} - \hat{i}_{qs}$.

In an adaptive observer, the stator resistance is estimated as

$$\hat{R}_s = -K_{rs}\int\left(e_{ids}\hat{\lambda}_{qr} + e_{iqs}\hat{\lambda}_{dr}\right)dt. \quad (6)$$

The control block diagram of adaptive observer including the stator resistance estimation is shown in Fig. 4.

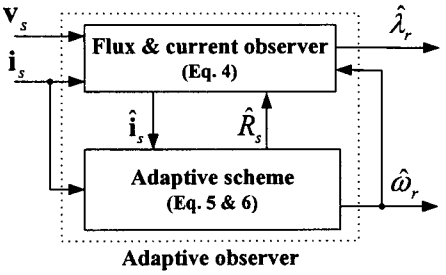

Fig. 4. Structure of the adaptive observer used in the sensorless control.

3. NONLINEAR MODELING OF MATRIX CONVERTER

The control structure shown in Fig.3 is using the measured the power grid voltages and the output current. The performance of the system is very dependent on

knowledge of output voltage and therefore the matrix converter has to be modeled. As in a voltage source converter influence on the commutation and voltage drop exists [4].

3.1 COMMUTATION DELAY

The switch commutation is an important issue when operating a matrix converter. When the current has to be commutated from one switch to another, it must be done in a four-step operation to avoid the circulating currents [1]. This strategy keeps both transistors turned on the switch while switch is conducting. As the current changes sign, the conducting diode, by nature, turns off, and the load current will be taken over by the opposite conducting branch.

Fig. 5 shows two subsequent commutations. The output voltage is shown with the control signals for the four transistor involved. In both cases the load current is positive and the input voltage, V2 is greater than V1. The conducting transistors are denoted by 1c and 2c whereas the non-conducting transistors are denoted by 1nc and 2nc.

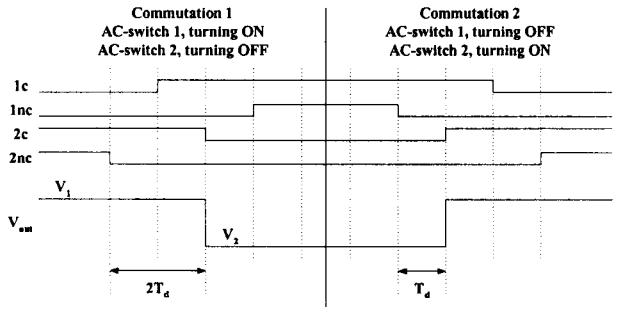

Fig. 5. Four-step commutation in a matrix converter

In Commutation 1, before the commutation process is started, the output voltage equals V_1. When the commutation process is terminated, the output voltage will be equal to V_1. As $V_2 > V_1$, the series diode in the positive conducting transistor in switch 1 is reverse biased, and no commutation takes place before the conducting transistor in switch 2 is turned OFF a T_d later. This results in a hard switched commutation. In Commutation 2, the polarity of the commutation voltage is opposite. The diode in the conducting branch of the ON-coming switch will be forward biased in the second step of the commutation process and a natural commutation will take place.

When the phase current i_{as} is positive, the turn-on and turn-off time error due to commutation delay is calculated from Fig. 5 as

$$T_{a,err} = T_d + T_f - T_r \tag{7}$$

where T_r is the rise time of the switching device and T_f is the fall time of the switching device.

In a similar way, the turn-on and turn-off time error when the phase current i_{as} is negative is calculated as

$$T_{a,err} = -(T_d + T_f - T_r). \tag{8}$$

From (7) and (8), these equations can be summarized as

$$T_{a,err} = (T_d + T_f - T_r)\,\mathrm{sgn}\,(i_{as}) \tag{9}$$

$$v_{a,cd} = \frac{T_{a,err}}{T_{sp}} v_{l-l} = v_{cd}\,\mathrm{sgn}\,(i_{as}) \tag{10}$$

where T_{sp} : switching period, v_{l-l} : line to line input voltage, and $v_{cd} = \dfrac{T_d + T_f - T_r}{T_{sp}} v_{l-l}$.

The voltage error due to commutation delay in each phase can be transformed to the stationary reference frame by employing the concept of the field orientation as

$$\begin{aligned}
\begin{bmatrix} v^s_{q.cd} \\ v^s_{d.cd} \end{bmatrix} &= \begin{bmatrix} \cos(0) & \cos\left(-\frac{2\pi}{3}\right) & \cos\left(\frac{2\pi}{3}\right) \\ \sin(0) & \sin\left(-\frac{2\pi}{3}\right) & \sin\left(\frac{2\pi}{3}\right) \end{bmatrix} \begin{bmatrix} v_{a,cd} \\ v_{b,cd} \\ v_{c,cd} \end{bmatrix} \\
&= v_{cd} \cdot \frac{2}{3} \begin{bmatrix} 1 & -\frac{1}{2} & -\frac{1}{2} \\ 0 & -\frac{\sqrt{3}}{2} & \frac{\sqrt{3}}{2} \end{bmatrix} \begin{bmatrix} \mathrm{sgn}\,(i_{as}) \\ \mathrm{sgn}\,(i_{bs}) \\ \mathrm{sgn}\,(i_{cs}) \end{bmatrix} \\
&= v_{cd} \begin{bmatrix} \frac{2}{3} & -\frac{1}{3} & -\frac{1}{3} \\ 0 & -\frac{\sqrt{3}}{3} & \frac{\sqrt{3}}{3} \end{bmatrix} \begin{bmatrix} \mathrm{sgn}\,(i^r_{qs}\cos(\theta_r)) \\ \mathrm{sgn}\left(i^r_{qs}\cos\left(\theta_r - \frac{2\pi}{3}\right)\right) \\ \mathrm{sgn}\left(i^r_{qs}\cos\left(\theta_r + \frac{2\pi}{3}\right)\right) \end{bmatrix}
\end{aligned} \tag{11}$$

3.2 ON-STATE SWITCHING DEVICE LOSS

The voltage drop in the matrix converter can be higher than that of the conventional inverter, and causes a severe disturbance at very low speed because two devices are all the time conducting. The threshold voltage of the power device has to be modeled to improve the low speed operation. If the forward voltage of the power devices can be approximated by a fixed-threshold value, v_{th}, the voltage drop across the power devices is general characterized as

$$v_d = R_d i_c + v_{th} \tag{12}$$

The resistance of the power device, R_d simplifies a linear relation between the load current and the inverter

voltage as shown in Fig. 6 and therefore it can be added to the value of the stator resistance. The value of R_d is estimated by (6).

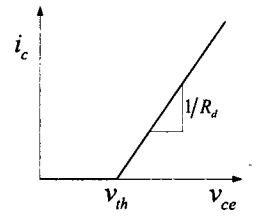

Fig. 6. Simplified forward on-state characteristics of the power device.

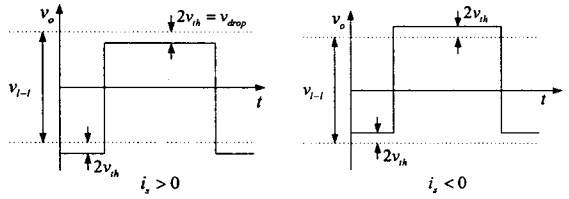

(a) (b)

Fig. 7. Simplified forward on-state characteristics of the power device (a) $i_s > 0$, (b) $i_s < 0$.

The on-state voltage drop is dependent on the direction of the phase current. Fig. 7 shows the voltage drop influence on the output voltage. The voltage drop in each phase can be transformed to the stationary reference as

$$\begin{bmatrix} v^s_{q,\,drop} \\ v^s_{d,\,drop} \end{bmatrix} = v_{drop} \begin{bmatrix} \frac{2}{3} & -\frac{1}{3} & -\frac{1}{3} \\ 0 & -\frac{\sqrt{3}}{3} & \frac{\sqrt{3}}{3} \end{bmatrix} \begin{bmatrix} \operatorname{sgn}\left(i^r_{qs}\cos(\theta_r)\right) \\ \operatorname{sgn}\left(i^r_{qs}\cos\left(\theta_r - \frac{2\pi}{3}\right)\right) \\ \operatorname{sgn}\left(i^r_{qs}\cos\left(\theta_r + \frac{2\pi}{3}\right)\right) \end{bmatrix} \tag{13}$$

where $v_{drop} = 2v_{th}$.

4. DESIGN OF DISTURBANCE OBSERVER USING RADIAL BASIS FUNCTION NETWORK

The mechanical system of the motor system can be represented as shown in Fig. 8.

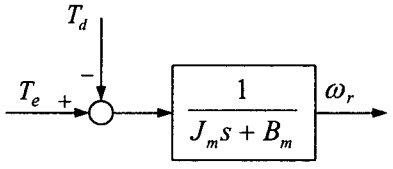

Fig. 8. Dynamic model of mechanical system

From the Fig. 8 using the estimated speed, $\hat{w}_r$, instead of the measured speed, w_r, the following equation (14) is obtained.

$$\dot{x}_q = A_n x_q + B_n u_m + C_n T_d \tag{14}$$

where $x_q = \hat{w}_r$, $A_n = -\frac{B_m}{J_m}$, $B_n = \frac{1}{J_m}$, $u_m = T_e$, and $C_n = -\frac{1}{J_m}$.

Eq. (14) is expressed by nominal values, but in most practical cases, inherent uncertainties in the induction motor model exist. Therefore, it is reasonable to assume that lumped uncertainties are presented in (15). From this, the following equation can be obtained.

$$\dot{x}_q = A_n x_q + B_n u_n + \epsilon \tag{15}$$

where $\epsilon = \Delta A_n x_q + \Delta B_n u_n + C_n T_d + \rho$,

ΔA_n and ΔB_n are modeling errors of A_n and B_n,

u_n is control input, and ρ is the unmodeled uncertainties.

In (15), if the uncertainties, ϵ, are exactly known, then the perfect control input for the closed loop system (15) to be asymptotically stable can be computed as

$$u_n = B_n^{-1}\left[\dot{x}_d - A_n x_q - \epsilon + K_x e_x\right] \tag{16}$$

where $e_x = x_d - x_q$, $x_d = w_r^*$ and K_x is design constant.

The next task is to replace the unknown uncertainties, ϵ, by the output of the RBFN and to develop an adaptation law for adjusting the parameters of the RBFN and controller for the purpose of forcing the tracking error to be zero under the lumped uncertainties.

The RBFN [7] is constructed with input, output and hidden layers of Gaussian activation functions. A schematic diagram of a simple type of RBFN is shown in Fig. 9, which consists of one input, one output and a single hidden layer. In general, the hidden nodes in the RBFN have normalized Gaussian activation function as:

$$z_q = \xi_q(x) \fallingdotseq \frac{\phi_q(x)}{\sum_k \phi_k(x)} = \frac{\exp\left[-|x - m_q|^2/2\sigma_q^2\right]}{\sum_k \exp\left[-|x - m_q|^2/2\sigma_k^2\right]} \tag{17}$$

where x is the input vector, m_q is the center, and σ_q is the width of q^{th} gaussian function.

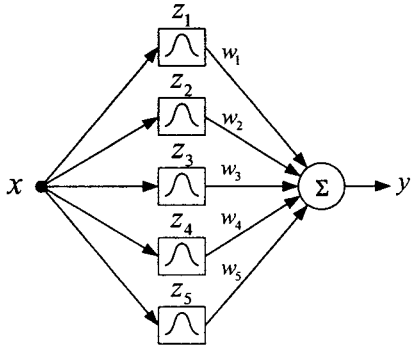

Fig. 9. Structure of the used RBFN

For each q^{th} hidden node, its receptive field, $\phi_q(x)$, is a region centered on m_q, and σ_q is the variance of the q^{th} Gaussian function. Therefore, a hidden node q gives a maximum response to input vectors close to m_q.

The output of the RBFN is simply the weighted sum of the hidden node output:

$$y = \sum_{q=1}^{l} w_q \cdot z_q = W^T \cdot Z = \epsilon \tag{18}$$

where w_i, $(i = 1, \cdots, l)$ are the weights between the i^{th} node and RBFN output, and $W \in R^n$ is the vector of $w_i's$.

If the RBFN disturbance observer perfectly identifies the unknown disturbances, the asymptotic stability of the whole system can be guaranteed. However, in the practical system, the reconstruction error is evitable. Thus an additional compensating control is required. Let the overall control input, u_q as

$$\begin{aligned} u_q &= u_n + u_p \\ u_p &= B_n^{-1}\zeta \mathrm{sgn}(e_x) \end{aligned} \tag{19}$$

where u_n is determined as (16) and u_p is an additional control for compensating the reconstruction error of the RBFN, ζ is the bounding constant, and sgn ($\cdot$) is the sign function.

In order to derive the adaptive law for the bounding constant, ζ, the weights of the RBFN, W, and compensating input, u_p, a *Lyapunov function* is defined in the following form:

$$V_e(t) = \frac{1}{2}e_x^2 + \frac{1}{2\gamma_W}(W - W^*)^T(W - W^*) + \frac{1}{2\gamma_\zeta}(\zeta - \zeta^*)^2 \tag{20}$$

where ζ^* is an optimal value of ζ.

The following adaptive scheme for the updating laws for the RBFN weight, W can be presented by the time derivative of the Lyapunov function to be a negative value.

$$\begin{aligned} \dot{W} &= -\gamma_W e_x Z, \\ \dot{\zeta} &= \gamma_\zeta |e_x|. \end{aligned} \tag{21}$$

The control block diagram of the proposed RBFN disturbance observer is then shown in Fig. 10.

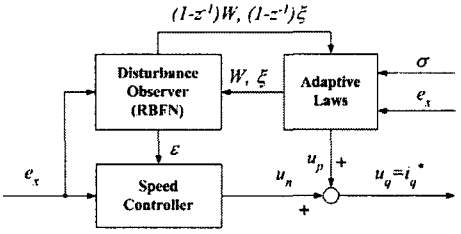

Fig. 10. Structure of the RBFN observer

5. EXPERIMENTS

To confirm the validity of the proposed control algorithm with all compensating methods, experiment is carried out. The robustness of the speed response against the parameter variation and load disturbance is especially focused on in the experiment. The experimental setup of the proposed control system consists of a 3-phase, 380 V, 60 Hz, 4 pole, 3 kW induction motor and power circuit using matrix converter. A dual controller system consisting of a 32-bit DSP (ADSP 21062) and a 16-bit microcontroller (80C167), in conjunction with a 12-bit A/D converter board is used to control the matrix converter based induction motor drive. The sampling time of control cycle is set at 150 μs for the proposed control algorithm.

Fig. 11 and Fig. 12 show experimental results of a sensorless vector controlled induction motor drive fed by matrix converter. Fig. 11 shows speed and phase current responses of the proposed sensorless vector control system in the forward and reverse operation. Fig. 12 shows a zoom of the zero-crossing in the speed response.

Fig. 13 shows distortion voltages as a function of the rotor position in the stationary reference frame. Fig 14 Fig. 16 show the experimental results of the current control with a non-linearity compensation at low speed

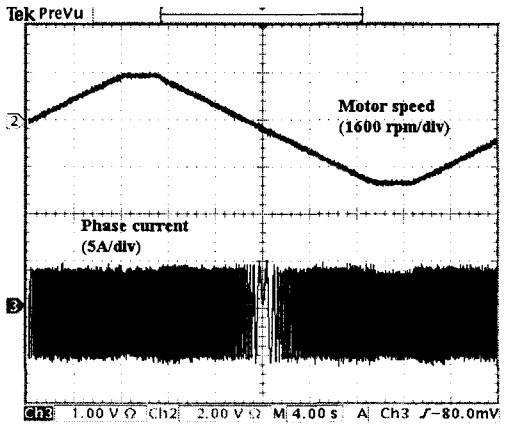

Fig. 11. Forward and reverse operation, experimental results; speed and phase current

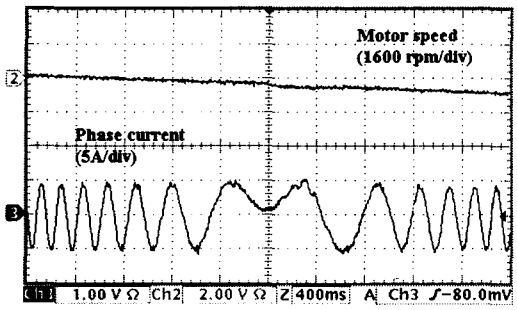

Fig. 12. A zoom of the zero crossing in Fig. 11; speed and phase current.

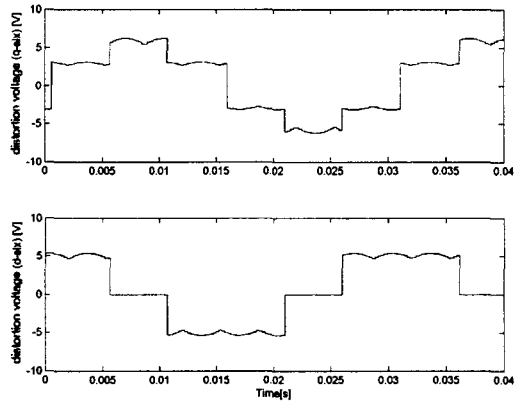

Fig. 13. Distortion voltages in the stationary reference frame (q- and d- axis distortion voltage).

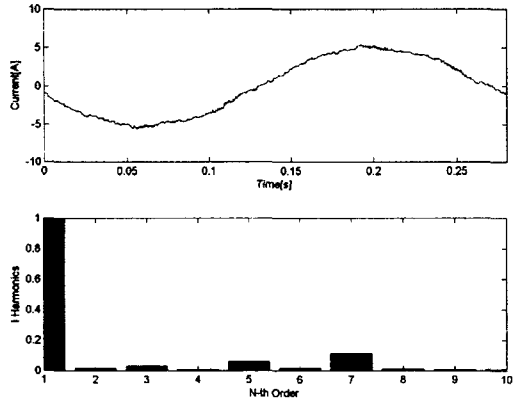

Fig. 14. Experimental results of current control without non-linearity compensation at 100 rpm (phase current and harmonic spectrum)

region. The motor is operated at 100 rpm in Fig. 14 and Fig. 15, and 5 rpm in Fig. 16. It can be seen that the current pulsations and their 5th and 7th harmonics are reduced using the proposed nonlinear modeling, and very good speed estimation is achieved at the low speed region down to 5 rpm Fig. 17 and Fig. 18 show the experimental results when the inertia value variation (50 % of the rated value) has occurred abrubtly. For speed control without RBFN disturbance observer, 1 s is taken

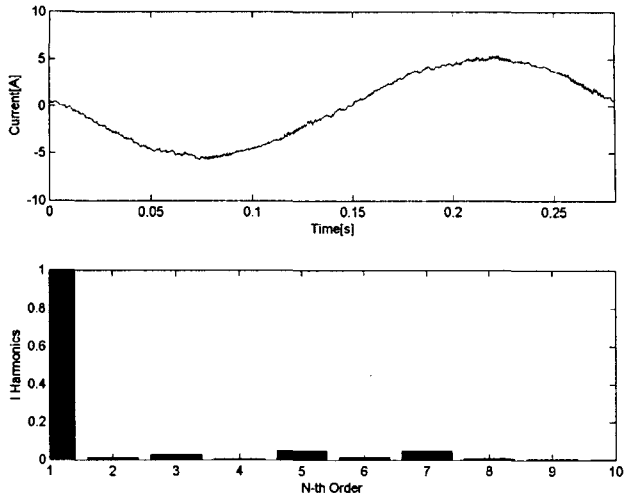

Fig. 15. Experimental results of current control with non-linearity compensation at 100 rpm (phase current and harmonic spectrum)

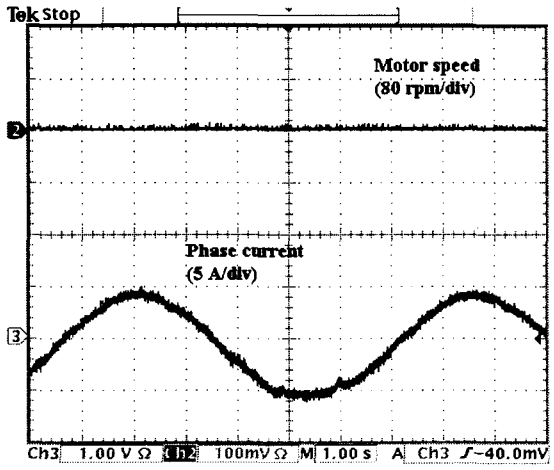

Fig. 16. Experimental results of constant speed operation at 5 rpm (speed and phase current)

to overcome the affection for the tracking error to be zero. However, speed control with RBFN disturbance observer has a robust characteristic against parameter variation.

This superiority can also be seen in Fig. 19 and Fig. 20. There is an abrubt load disturbance (50 % of the rated value) at 5 s. For the speed control with RBFN control, it takes about 0.5 s for the tracking error to be zero, but the speed control without the RBFN observer uses 2 s. From these experimental results, the best speed control characteristics in the sensorless vector control system are observer when the lumped disturbances exist. Especially, the proposed control scheme has robust characteristics against parameter variation even though there is a negligible external disturbance effect.

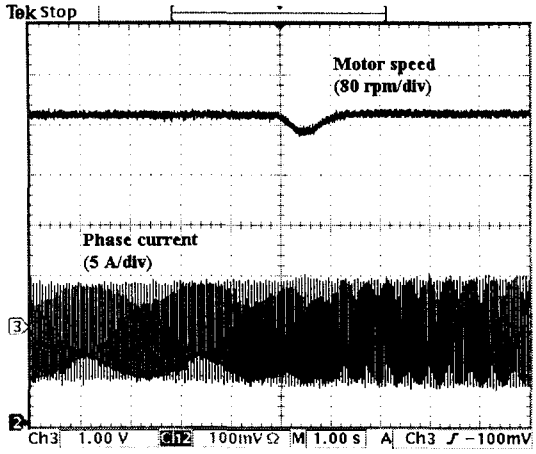

Fig. 17. Experimental results of the parameter variation without RBFN disturbance observer at 500 rpm (speed and phase current)

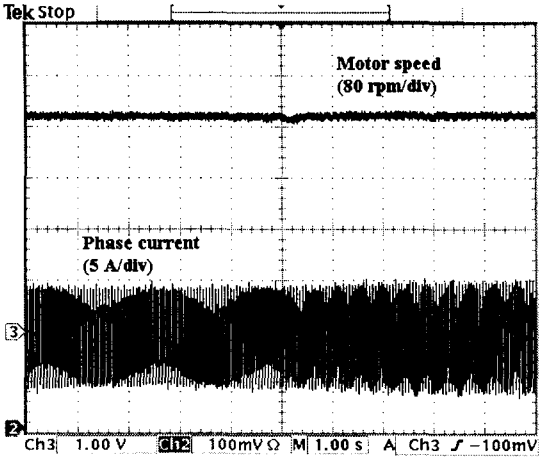

Fig. 18. Experimental results of the parameter variation with RBFN disturbance observer at 500 rpm (speed and phase current)

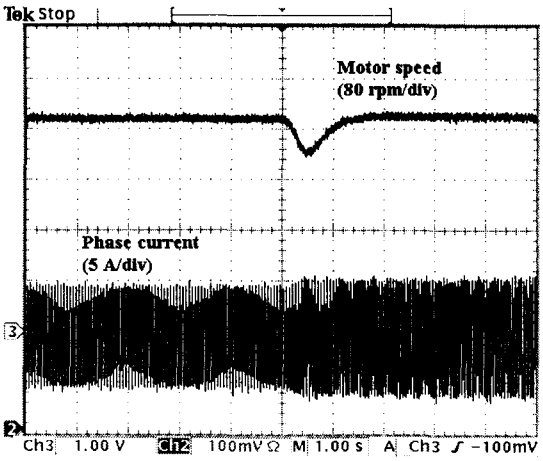

Fig. 19. Experimental results of load disturbance without RBFN disturbance observer at 500 rpm (speed and phase current)

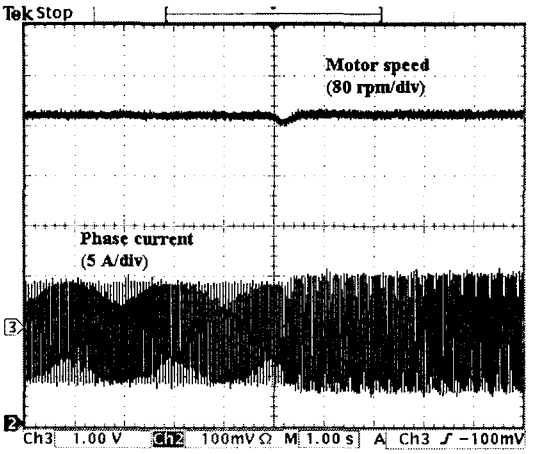

Fig. 20. Experimental results of load disturbance with RBFN disturbance observer at 500 rpm (speed and phase current)

6. CONCLUSION

In order to realize high performance control of induction motor drives fed by matrix converter, a new matrix converter model for low speed operation and robust speed controller using a disturbance observer have been proposed in this paper. The nonlinear voltage distortion that is caused by commutation delay and on state voltage drop in the power device is corrected by a simple feed-forward compensation method using the direction of current. In addition, to achieve a robust control characteristic against unmodeled disturbances such as parameter variations and load disturbances, the unmodeled disturbances are approximated by the radial basis function network. Experimental results show that the proposed control scheme can provide good performance at the low speed region and robust and stable characteristics against parameter variations and load disturbance.

ACKNOWLEDGMENT

This work was supported by the Post-doctoral Fellowship Program of Korea Science & Engineering Foundation (KOSEF).

REFERENCES

[1] P. Nielsen, F. Blaabjerg, and J. K. Pedersen "New Protection Issues of a Matrix Converter," IEEE Trans. Industry Applications, vol. 35, no. 5, Sep./Oct. 1999, pp. 1150-116.

[2] C. Klumpner, P. Nielsen, I. Boldea, and F. Blaabjerg,

"A New Matrix Converter-Motor (MCM) for Industry Applications," IEEE Trans. Industrial Electronics, vol. 49, no. 2, April 2002, pp. 325-335.

[3] M. P. Kazmierkowski, R. Krishnan, and F. Blaabjerg, Control in power electronics-selected problems. Academic press, 2002, ISBN 0-12-402772-5, ch. 3.

[4] F. Blaabjerg, J. K. Pedersen, and P. Thoegersen "Improved Modulation Techniques for PWM-VSI Drives," IEEE Trans. Power Electronics, vol. 44, no. 1, Feb. 1997, pp. 87-95.

[5] J. Holtz, "Sensorless Control of Induction Motor Drives," Proc. of the IEEE, vol. 90, no. 8, Aug. 2002, pp. 1359-1394.

[6] Kyo-Beum Lee, Joong-Ho Song, Ick Choy, Kwang-Bae Kim, and Ji-Yoon Yoo, "An Improvement on low Speed Operation Performances of DTC for 3-level Inverter-fed Induction Motors," Trans. KIEE. vol. 49B, No. 10, pp. 693-700, Oct., 2000 (in Korean).

[7] H. S. Huh, K. B. Lee, J. H. Park, I. Choy, and G. T. Park, "Design of a Robust Stable Speed-Sensorless Induction Motor Direct Torque Control System Using the RBFN," Proc. of PESC03, 2003, pp. 580-585.

저 자 소 개

이 교 범(李 教 範)

He was born in Seoul, Korea, in 1972. He received the B.S. and M.S. degrees in electrical and electronic engineering from the Ajou University, Korea, in 1997 and 1999, respectively. He received the Ph.D. degrees in electrical engineering from the Korea University, Korea in 2003.

Since 2003, he has been with the Institute of Energy Technology as a Post Doc. researcher in Aalborg University, Denmark. His research interests include electric machine drives and power electronics.

Tel : +45 9635-9283

Fax : +45 9815-1411

E-mail : kyl@iet.auc.dk